Formation of Planar and Spiral Ca^{2+} Waves in Isolated Cardiac Myocytes

Hideyuki Ishida,* Chokoh Genka,* Yuki Hirota,# Hiroe Nakazawa,* and William H. Barry§

*Department of Physiology, School of Medicine, Tokai University, Bohseidai, Isehara, Kanagawa, Japan; the #Electro-Chemical and Cancer Institute, Kokuryo-cho, Chofu, Tokyo, Japan; and the §Division of Cardiology, University of Utah Health Sciences Center, Salt Lake City, Utah 84132 USA

ABSTRACT A novel Nipkow-type confocal microscope was applied to image spontaneously propagating Ca^{2+} waves in isolated rat ventricular myocytes by means of fluo-3. The sarcolemma was imaged with di-8-ANEPPS and the nucleus with SYTO 11. Full frame images in different vertical sections were obtained at video frame rate by means of an intensified CCD camera. Three types of Ca^{2+} waves were identified: spherical waves, planar waves, and spiral waves. Both spherical waves and spiral waves could initiate a planar wave, and planar waves were not influenced by the presence of a nucleus. Spiral waves, however, were consistently found adjacent to a nucleus and displayed a slower propagation rate and slower rate of increase in Ca^{2+} concentration in the wave front than did spherical and planar waves. The planar waves were apparent throughout the vertical axis of the cell, whereas spiral waves appeared to have a vertical height of approximately 3 μm, less than the maximum thickness of the nucleus (5.0 $\pm$ 0.3 μm). These results provide experimental confirmation of previous modeling studies which predicted an influence of the nucleus on spiral-type Ca^{2+} waves. When a spontaneous Ca^{2+} wave is small relative to the size of the nucleus, it appears that the Ca^{2+} buffering by the nucleus is sufficient to slow the rate of spontaneous propagation of the Ca^{2+} wave in close proximity to the nucleus. These findings thus support the idea that the nucleus can influence complex behavior of Ca^{2+} waves in isolated cardiac myocytes.

INTRODUCTION

Ca^{2+}-induced Ca^{2+} release (CICR) is the basis for the excitable behavior and subsequent contraction of cardiac myocytes (Cannell et al, 1995; Fabiato and Fabiato, 1975; Lopez Lopez et al., 1995; Niggli and Lederer, 1990b; Wier, 1993; Wong et al., 1992). CICR is also very apparent in other less physiological conditions when isolated cardiomyocytes spontaneously exhibit Ca^{2+} waves under voltage clamp (Takamatsu and Wier, 1990) or when they are overloaded with Ca^{2+} (Lipp and Niggli, 1993). Propagating Ca^{2+} waves in cardiac myocytes have in the past been described as planar waves which travel along the longitudinal cell axis. However, recent observations performed by confocal microscopy have demonstrated other complex patterns of Ca^{2+} wave propagation, such as spiral Ca^{2+} waves (Lipp and Niggli, 1993; Engel et al., 1994).

Spatially complex propagation phenomena have been predicted by mathematical models in a variety of systems exhibiting positive feedback (Gerhardt et al., 1990; Fast et al., 1990). Lipp and Niggli (1993) demonstrated that complex patterns of Ca^{2+} wave propagation can be influenced by positive feedback, most likely the CICR mechanism. Lipp et al. (1996) also suggested that a region of inhomogeneity in positive feedback, such as the nucleus, may be responsible for complex patterns of the Ca^{2+} wave. Recently, Dupont et al. (1996) modeled spiral Ca^{2+} waves by numerical simulations. In their simulations, a spiral Ca^{2+} wave could occur as a result of the spatial heterogeneity created by the nucleus, a region lacking a releasable Ca^{2+} pool. It is known that spiral waves are also most often observed near a nucleus (Lipp and Niggli, 1993). Thus, the two-dimensional studies of Lipp and Niggli (1993) and the modeling work of Dupont et al. (1996) imply that a spiral Ca^{2+} wave can be initiated by a nucleus.

Two-dimensional studies cannot examine the propagation of a Ca^{2+} wave in the vertical axis, although this could be important as Ca^{2+} waves propagate in all directions (Wussling and Salz, 1996). For example, a spiral Ca^{2+} wave could be caused by a nucleus provided that the size of the Ca^{2+} wave in the vertical axis is smaller than the diameter of nucleus. If the size of a Ca^{2+} wave in the vertical axis is larger than the diameter of the nucleus, the arrival of the Ca^{2+} wave at the opposite sides of the nucleus in the transverse direction may be nearly simultaneous, resulting in a more uniform propagation. Thus, examination of propagation of a Ca^{2+} wave in the vertical axis is important, but three-dimensional observation of Ca^{2+} waves has not been carried out.

Conventional confocal microscopes using line scan systems have a great advantage over ordinary optical microscopes in that they reject light that does not come from the focal plane. A semi-confocal system using a slit scan method allows scan of 512 $\times$ 480 pixels with high temporal resolution (Wussling et al., 1996). However, full frame/real-time imaging using a one-pinhole scanning method is difficult. On the other hand, spinning disk confocal microscopes have the advantage of being able to observe full frame/real-time images. However, because light transmission through the disk is usually less than 5%, weakly fluorescent specimens are difficult to image. We have developed a novel Nipkow disk confocal microscope which

Received for publication 9 March 1999 and in final form 2 July 1999.

Address reprint requests to Hideyuki Ishida, PhD, Dept. of Physiology, School of Medicine, Tokai University, Bohseidai, Isehara, Kanagawa 259-1193, Japan, Tel.: +81-463-93-1121(2534); Fax: +81-463-93-6684; E-mail: ishida@is.icc.u-tokai.ac.jp.

0006-3495/99/10/2114/09 $2.00

has 20,000 pinholes each with a microlens. The addition of the microlens on the pinholes increases light transmission through the disk by 40% (Ichihara et al., 1999; Genka et al., 1999). The aim of the present study was to use the novel Nipkow disk confocal microscope to investigate with three-dimensional observations how planar and spiral Ca^{2+} waves in cardiac myocytes are influenced by a nucleus.

MATERIALS AND METHODS

Cell preparation and solutions

Animals were maintained and used according to both the National Institutes of Health Guidelines for Laboratory Animal Care and the Animal Care Protocol of Tokai University.

Cardiac myocytes from rat ventricles were prepared by standard methods (Kagaya et al., 1995). Briefly, following anesthesia (pentobarbital, 100 mg/kg), the heart was removed from the chest and perfused retrograde via the aorta using the Lagendorff method. The basic perfusate (solution A; nominally Ca^{2+}-free) contained (mM): NaCl, 137; Hepes, 5; dextrose, 22; taurine, 20; creatine, 5; KCl, 5.4; $MgCl_2$, 1; sodium pyruvate, 5. It was titrated to a pH of 7.4 with NaOH. The heart was perfused at 37°C with solution A for 5 min. After this, the heart was perfused for about 20 min with solution A plus 0.1 mM Ca^{2+} with 0.5 mg/ml collagenase (Type II, Worthington, Freehold, NJ). The enzyme was then washed out by perfusing with solution A plus 0.1 mM Ca^{2+} for 5 min. The left ventricle was removed from the heart, chopped into small pieces, and then shaken at 37°C for 10 min in a glass conical flask containing 50 ml of solution A plus 0.1 mM Ca^{2+}. The cell suspension was filtered (200 μm mesh), sedimented in a 50-ml glass beaker for 5 min, and the supernatant then replaced with a higher Ca^{2+}-containing solution; the Ca^{2+} was increased in three steps up to 1 mM. The single cells were kept with 47.5% solution A, 47.5% medium 199, and 5% FCS at room temperature until use (up to 4 h).

Imaging of t-tubules, nuclei, and Ca^{2+} waves

The nucleus was stained with SYTO 11 (0.5 μM, Molecular Probes, Eugene, OR), and t-tubules were stained with the voltage-sensitive dye di-8-ANEPPS (10 μM, Molecular Probes). We observed Ca^{2+} wave propagation using fluo-3 loaded into cells by exposure to 10 μM fluo-3 AM (Molecular Probes). Cells were exposed to dyes for 30 min at 37°C. Myocytes were exited at 488 nm with light from an argon laser, and fluorescence at 530 nm was detected via a barrier filter.

Nipkow disk confocal microscope

Fig. 1 shows a schematic diagram of the construction of the Nipkow disk confocal system. This system was based on the Nipkow disk and Tandem scanner (Nipkow, 1884; Petran et al., 1968). Our system has two disks; an upper disk has 20,000 microlenses which focus the excitation light (488-nm Argon laser; 2013 Uniphase, San Jose, CA) on 20,000 corresponding pinholes in the lower disk. The upper disk was mechanically connected to the lower disk, and both disks were rotated by a motor at 1800 rpm. The microlenses increase light transmission to about 40% of the light from the source. The passed light was focused by an objective lens (×100, n.a. 1.3, Zeiss) on a plane in a specimen. Fluorescence emission light from the specimen returned along the same path through the objective lens and pinholes. The emission light was reflected by a dichroic mirror and then was imaged through a relay lens to an intensified CCD camera (SR UB GEN III+, Solamere, Salt Lake City, UT).

Measurement of propagation velocity

To determine wave velocity, we measured at each frame the position of the front of a Ca^{2+} wave, defined to be the point at which the increasing fluorescence intensity reached a half-maximum value (Wussling et al., 1996). The propagation velocity was estimated from serial frames as propagation length/time.

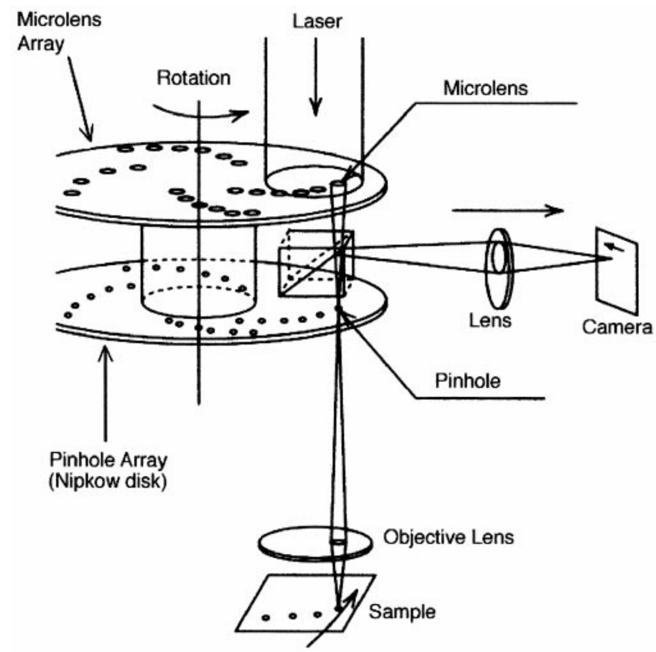

FIGURE 1 Schematic diagram of the Nipkow disk confocal system. (From Ichihara et al., 1999 with permission).

Vertical positioning mechanism

The confocal sections in the vertical axis were selected by movement of the calibrated vertical vernier control on the microscope in ~1-μm increments.

Image processing

A LG-3 frame-grabber board (Scion, Frederick, MD) with National Institutes of Health Image 1.61 software running on a Power Macintosh 8500/120 computer was used for the digitization of video frames.

RESULTS

Size of nucleus in transverse section

To examine the potential of the nucleus to obstruct Ca^{2+} waves, we measured the size of the nucleus relative to that of ventricular myocytes in the transverse and vertical axes. Fig. 2 shows optical slice images and reconstruction of these slice images. A rat ventricular myocyte was labeled with di-8-ANEPPS (t-tubules) and SYTO 11 (nucleus) was sliced at 1-μm increments using the Nipkow disk confocal microscope (Fig. 2 *A*). These longitudinal and transverse cross-section images were reconstructed along the vertical axes by computer (Fig. 2 *B*). The length of the cells averaged 100.1 ± 2.6 μm (n = 11), the width 27.8 ± 0.9 μm (n = 11), and the depth 12.4 ± 1.3 μm (n = 6). The diameter and maximum thickness of the nucleus averaged 20.5 ± 1.3 and 5.0 ± 0.3 μm, respectively. Thus, the

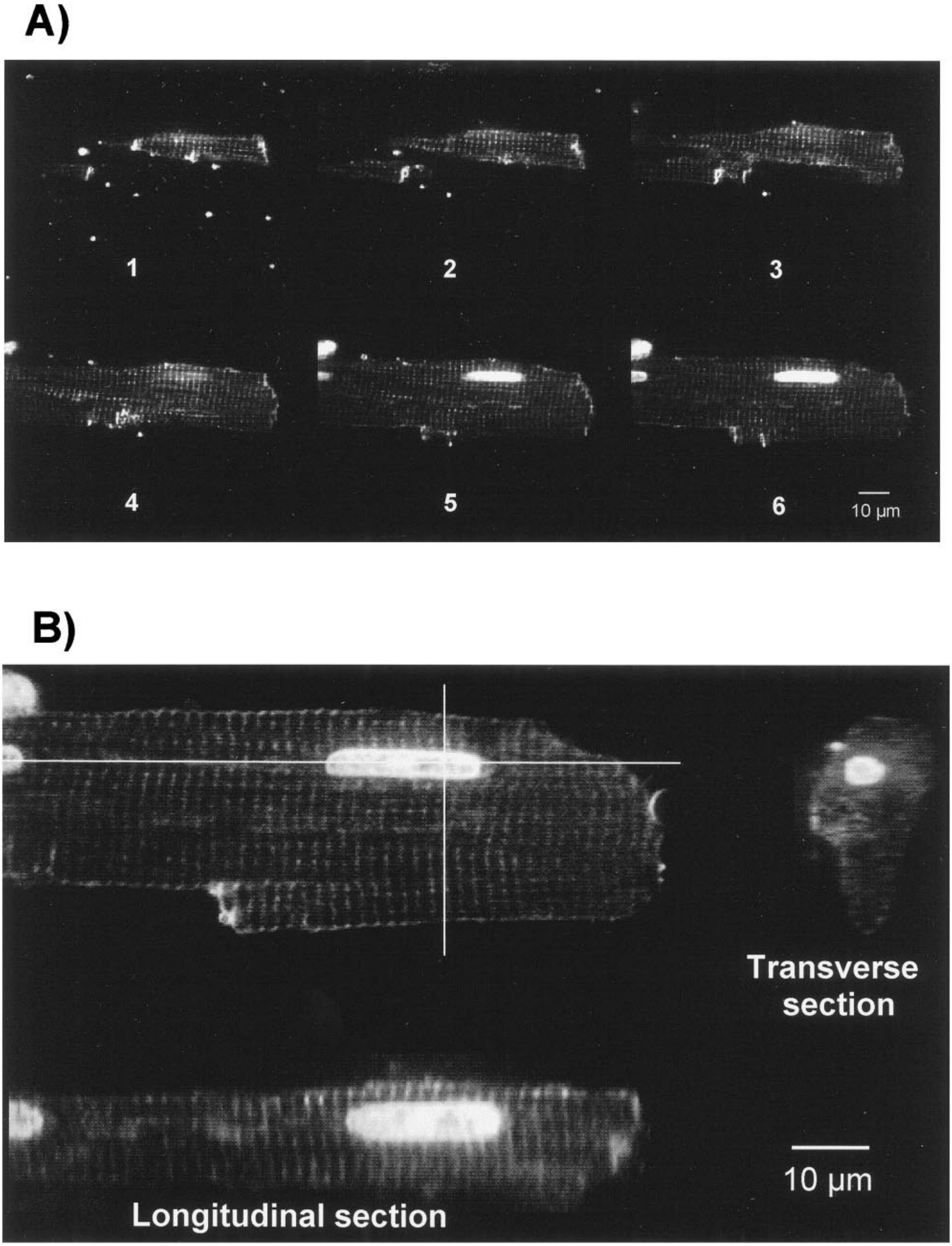

FIGURE 2 Optical slice images and reconstructions from these slice images. A rat cardiac myocyte labeled with di-8-ANEPPS (t-tubules) and SYTO 11 (nucleus) was sliced at 1 μm thickness intervals by Nipkow disk confocal microscopy. *A* shows 6 of 16 sliced images. The reconstructions of 16 images into longitudinal and transverse cross-sections were produced by computer and are shown in *B*.

nucleus occupies a significant proportion of the cell depth and could be expected to present a significant obstacle to the propagation of Ca^{2+} waves.

Development of planar and spiral Ca^{2+} waves

Fig. 3 shows the development of a planar Ca^{2+} wave from a spherical Ca^{2+} wave in a cardiac myocyte. In the first frame in which an increase in Ca^{2+} was observed (0 ms) in Fig. 3, we see a Ca^{2+} wave starting from a point at the lower left end of the cell. The Ca^{2+} wave expanded as a spherical Ca^{2+} wave (Fig. 3, *top* and *center*; 33–165 ms). After the Ca^{2+} wave arrived at the other side of cell membrane, the spherical Ca^{2+} wave changed to a planar Ca^{2+} wave (165 ms in Fig. 3). The planar Ca^{2+} wave traveled along the longitudinal cell axis (Fig. 3, *bottom*). As shown at 462 ms in Fig. 3, the propagation of the planar Ca^{2+} wave was not blocked by a nucleus. The average velocity of the planar waves was 92 $\pm$ 8 μm/s (n = 11, mean $\pm$ S.E.M.).

Fig. 4 shows a development of a planar Ca^{2+} wave from a spiral Ca^{2+} wave. In the first panel in which an increase in Ca^{2+} occurred (0 ms) in Fig. 4, we see a Ca^{2+} wave starting near a nucleus, at the upper left end of the cell. The Ca^{2+} wave propagated from the left side to the center of the cell along the nucleus as a spiral Ca^{2+} wave (Fig. 4, *top* and *center*; 33–165 ms). The spiral Ca^{2+} wave increased in size and intensity at 165 ms. In Fig. 4 *bottom* (264–462 ms), we observed that the Ca^{2+} wave separated into two types of Ca^{2+} waves: one a spiral wave which propagated around the left nucleus, and a planar wave moving to the right. The right nucleus did not block the planar Ca^{2+} wave (Fig. 4; 462 ms). The average velocity of spiral waves was 36 $\pm$ 4

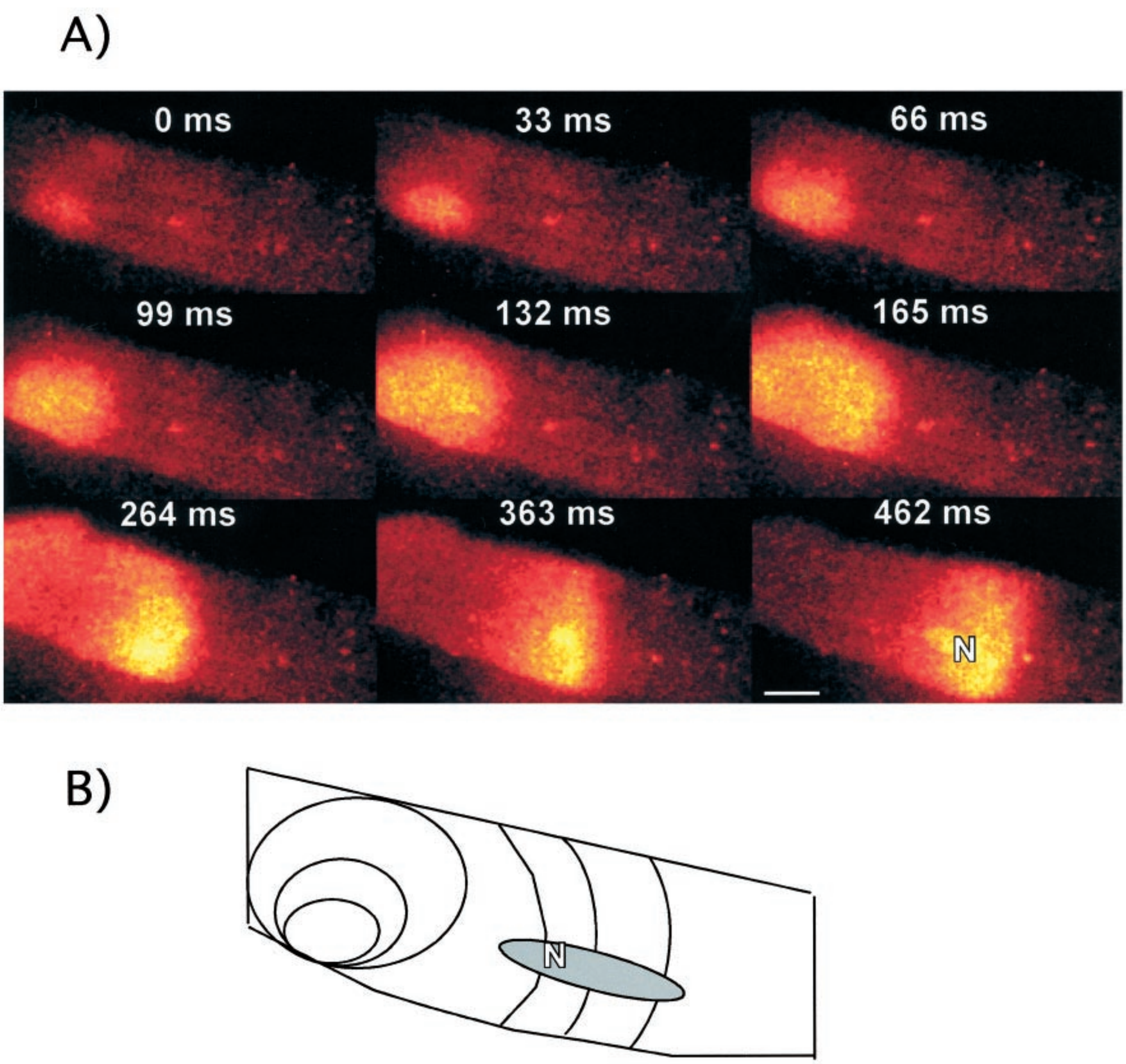

FIGURE 3 Two-dimensional depiction of planar Ca^{2+} wave revealed by Nipkow confocal microscopy. (*A*) A sequence of fluorescence images shows development of a planar Ca^{2+} wave from a spherical Ca^{2+} wave. The optical section is about 0.5 μm thick. The spatial extension of the wave along the vertical axis of the cell ensures that the waves are at least partially in the focal plane and cannot intermittently escape confocal detection. The nucleus is shown in the 462 ms panel as N. *Scale bar* = 10 μm. (*B*) The propagating pattern of planar Ca^{2+} wave is shown. Similar results were observed in eight experiments.

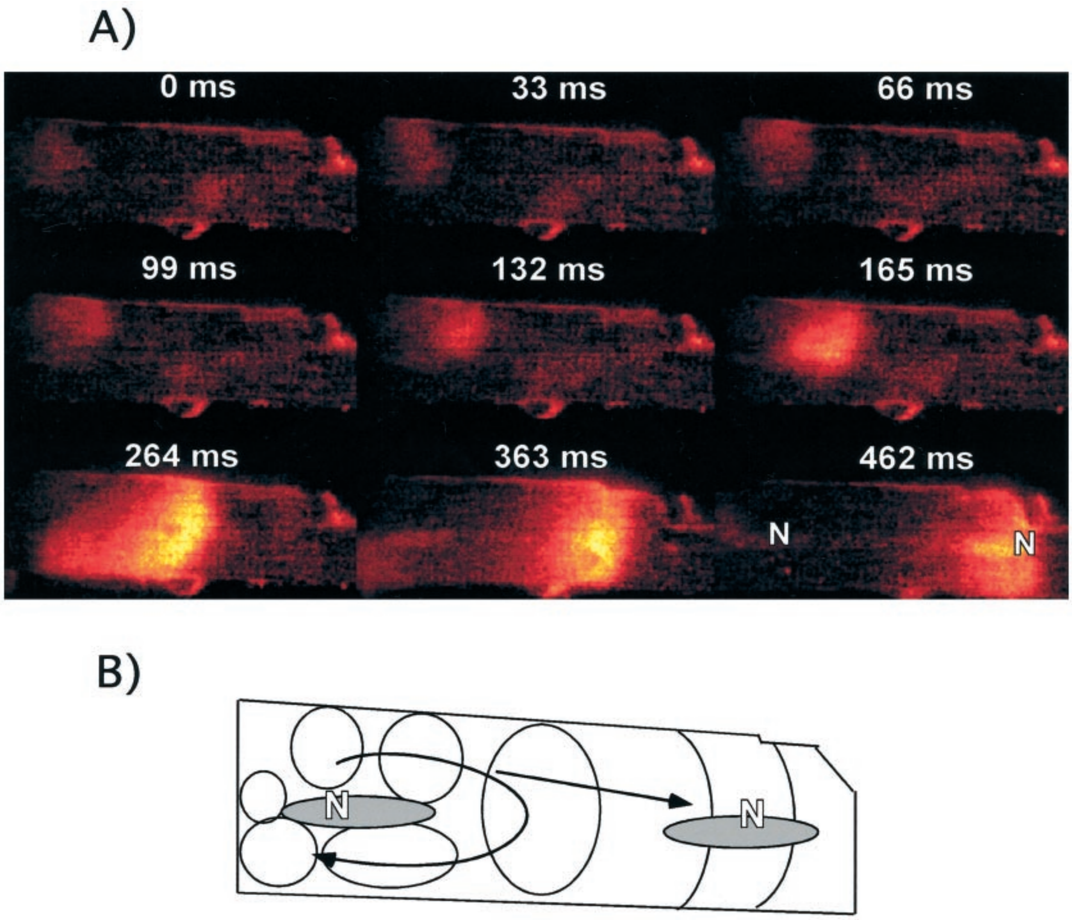

FIGURE 4 Two-dimensional detection of a spiral Ca^{2+} wave by Nipkow confocal microscopy. (*A*) A sequence of fluorescence images shows a development spiral Ca^{2+} wave. The nuclei are shown in the 462 ms panel as N. *Scale bar* = 10 μm. (*B*) The propagating pattern of spiral and planar Ca^{2+} waves is shown. Images representative of results in three experiments.

μm/s (n = 4, mean ± S.E.M.). These results indicate that the nucleus influences the propagation of a spiral Ca^{2+} wave but not a planar Ca^{2+} wave.

To evaluate further the differences between planar and spiral Ca^{2+} waves, we measured the rate of changes in the fluo-3 fluorescence intensity at the center of Ca^{2+} waves

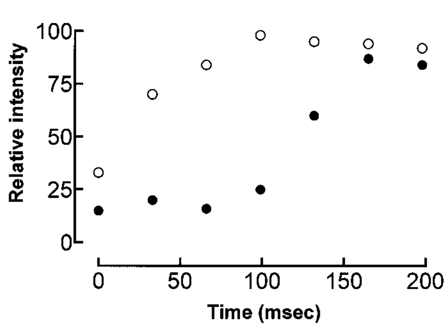

FIGURE 5 Time course of change in intensity of fluorescence during Ca^{2+} waves. *Open circles* indicate the planar wave in Fig. 3 and *solid circles* indicate the spiral wave in Fig. 4. The resting Ca^{2+} level was assigned a value of 0 and the maximum Ca^{2+} a value of 100.

shown in Fig. 3 and in Fig. 4. As shown in Fig. 5, in the planar Ca^{2+} wave, the Ca^{2+} concentration in the Ca^{2+} wave increased with time and saturated at 99 ms after starting (*open circles*). On the other hand, the development of a rapid rate of Ca^{2+} concentration increase in a spiral Ca^{2+} wave was relatively delayed (Fig. 5, *solid circles*). This result suggests that Ca^{2+} concentration does not increase rapidly during propagation of a spiral Ca^{2+} wave near a nucleus. Moreover, as described above, the propagating speed of spiral Ca^{2+} waves was slower than that of planar Ca^{2+} waves (36 ± 4 and 92 ± 8 μm/s, respectively). This result also is consistent with the observation that the rate of increase in Ca^{2+} concentration in a spiral Ca^{2+} wave is lower than in a planar Ca^{2+} wave.

Propagation of Ca^{2+} waves at different vertical points

Fig. 6 shows that a propagation of a planar Ca^{2+} wave from right to left could be observed at six different vertical sections. This result indicates that a planar Ca^{2+} wave propagates relatively uniformity in the vertical axis, consis-

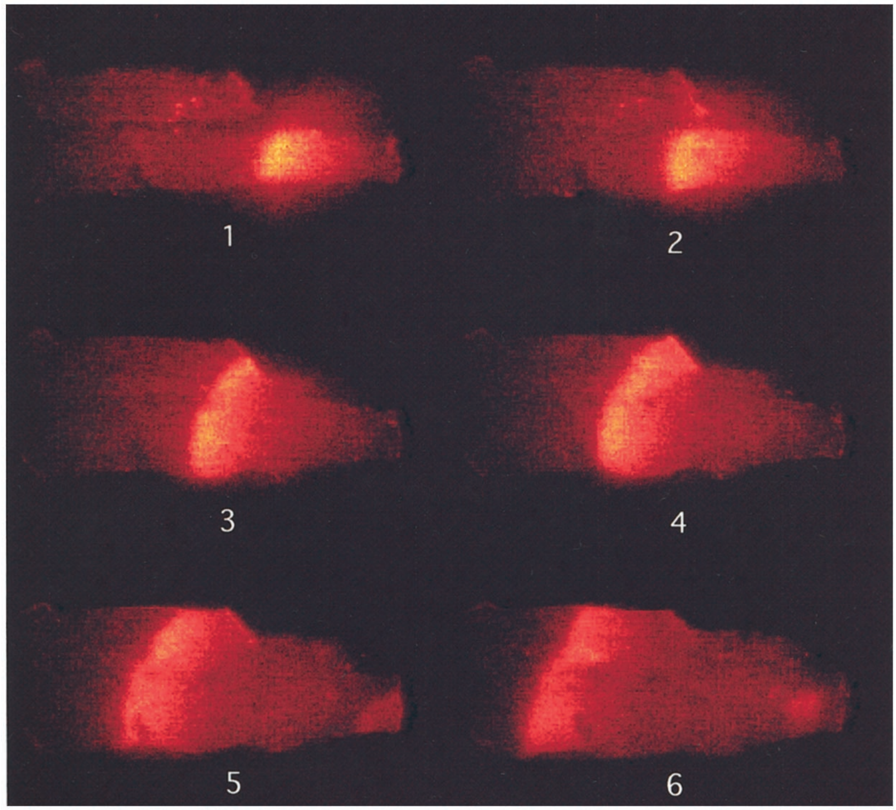

FIGURE 6 Propagation of a planar Ca^{2+} wave at different vertical sections. Ca^{2+} propagation was observed at 1-μm changes in the vertical axis (*panels 1–6*). Similar results were obtained in seven different cells.

tent with the idea that a planar Ca^{2+} wave propagates above and below a nucleus.

In Fig. 7 is shown a similar analysis of a spiral wave. Propagation of spiral Ca^{2+} wave from the upper right side was observed in the initial vertical section (Fig. 7 *A*). However, when this wave was imaged in different vertical sections (Fig. 7 *B*), it was observed in only two sections (*panels 3* and *4*). (Each section 1–6 in *B* is separated by about 1 μm in vertical axis). This result indicates that the vertical size of a spiral Ca^{2+} wave is less than diameter of the nucleus (Fig. 2; 5 μm) and is consistent with the idea that a spiral Ca^{2+} wave can be blocked by a nucleus in the vertical axis.

DISCUSSION

We have developed a Nipkow-type disk confocal microscope which permits observation of three-dimensional images of living cells at 33 full frames/s with high signal-to-noise ratio (Ichihara et al., 1999). Applying this confocal microscope to detect $[Ca^{2+}]_i$ by fluo-3 fluorescence, we have investigated spontaneously occurring spherical, planar, and spiral Ca^{2+} wave characteristics in three dimensions in rat ventricular myocytes.

In cardiac myocytes, a Ca^{2+} wave is driven by the CICR mechanism. The velocity of a propagating Ca^{2+} wave is determined by the amount of released Ca^{2+}, the distribution of release sites, and the diffusion coefficient of Ca^{2+} in the cytosolic space (Fabiato, 1985; Stern et al., 1988; Ishide et al., 1992) and has been reported to range from 80 to 120 μm/s (Stern, 1992). The velocity of planar waves that we observed (91 μm/s) falls within this range. However, various mechanisms may alter Ca^{2+} waves. Tang and Othmer (1994) predicted a velocity of Ca^{2+} waves in cardiac myocytes of 81 μm/s, assuming a diffusion coefficient for Ca^{2+} in the cytoplasm of 5.0×10^{-4} mm^2/s. This is considerably less than the measured diffusion coefficient for Ca^{2+} in oocyte cytoplasm ($13–65 \times 10^{-3}$ mm^2/s; Allbritton et al., 1992). However, buffering of Ca^{2+} by cytosolic proteins may be stronger in myocytes than oocytes, and, as Tang and Othmer point out, the wave velocity is dependent also on Ca^{2+} release channel dynamics. Thus a reduction in Ca^{2+} release sites as well as altered Ca^{2+} buffering might have a marked effect on wave velocity.

Obstacles may also contribute to the complexity of Ca^{2+} waves. Recently, Dupont et al. (1996) simulated Ca^{2+} waves and proposed that spiral Ca^{2+} waves can occur as a result of the spatial heterogeneity created by the nucleus, which is a region lacking a releasable Ca^{2+} pool. Consistent with their hypothesis, we observed that spiral Ca^{2+} waves were initiated near a nucleus (Fig. 4). This observation is also consistent with the previous observations (Lipp and Niggli, 1993). Therefore, we focused our study on the influence of the nucleus on planar and spiral Ca^{2+} waves.

Ca^{2+} waves may expand in all directions. Our three-dimensional observations clearly demonstrated that the planar Ca^{2+} wave propagated horizontal (X-Y direction) and vertical directions (Figs. 3 and 6). The planar Ca^{2+} wave

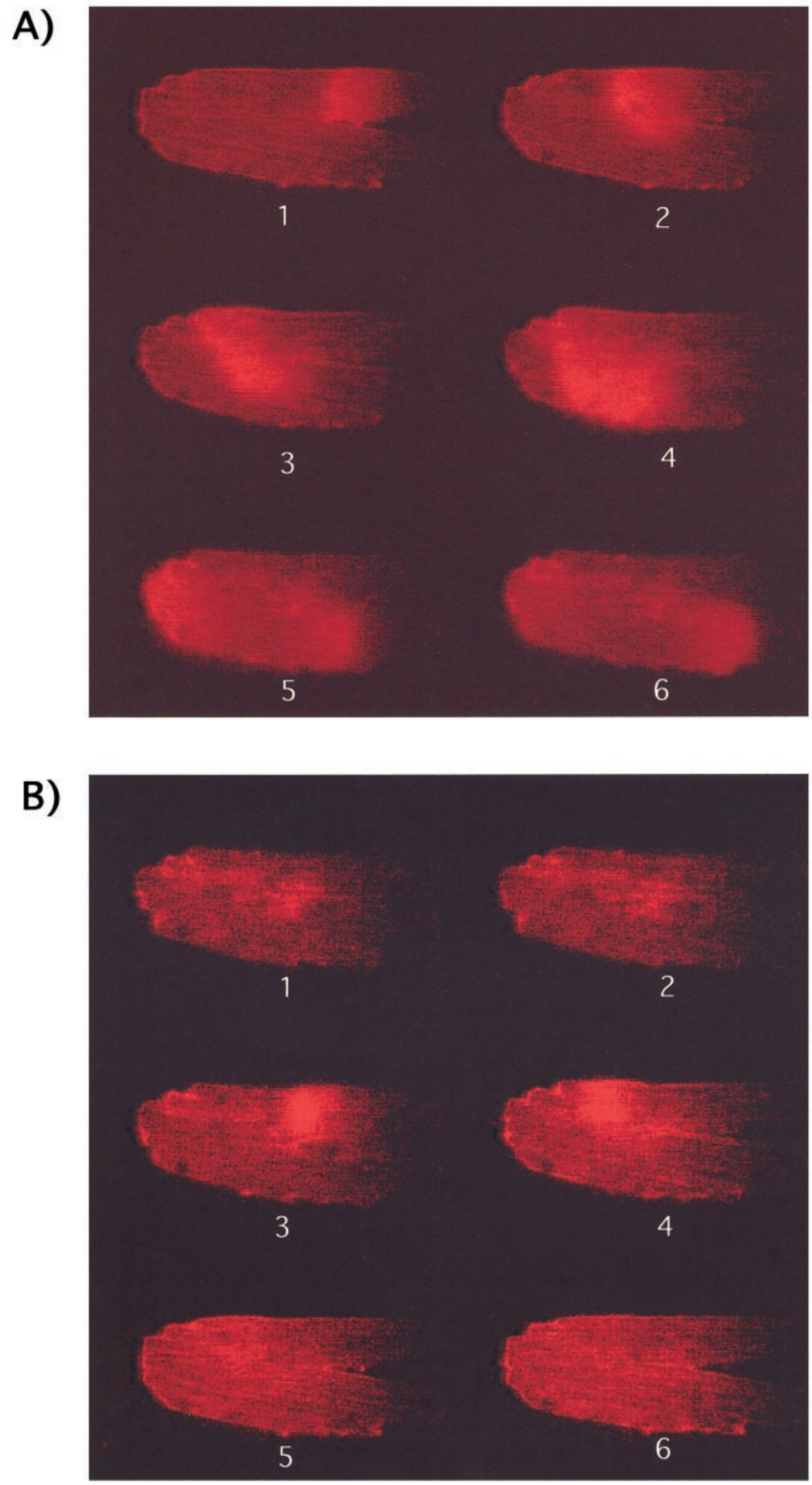

FIGURE 7 Propagation of spiral Ca^{2+} wave at different vertical sections. (*A*) A spiral Ca^{2+} wave is observed in the same vertical section. (*B*) Ca^{2+} propagation in a spiral Ca^{2+} wave is observed in different vertical sections. Each numbered panel differs about 1 μm in vertical axis. This experiment is representative of findings in four different cells.

could propagate above, below, and around a nucleus. Therefore, it appears that the nucleus does not block the propagation of a planar Ca^{2+} wave (see 462 ms panel in Fig. 3 and 462 ms panel in Fig. 4). On the other hand, spiral Ca^{2+} waves propagated around the nucleus (Fig. 4) and the propagation velocity of a spiral Ca^{2+} wave was consistently slower than that of a planar Ca^{2+} wave. Also, the Ca^{2+} concentration increased slowly on the leading edge of a spiral Ca^{2+} wave (Fig. 5).

A large change in local Ca^{2+} concentration is needed to induce Ca^{2+} release of adjacent RyR channels in a propagating Ca^{2+} wave. Therefore, the smaller size and lower concentration of spiral Ca^{2+} wave is assumed to be due to at least three factors: a low Ca^{2+} store in sarcoplasmic

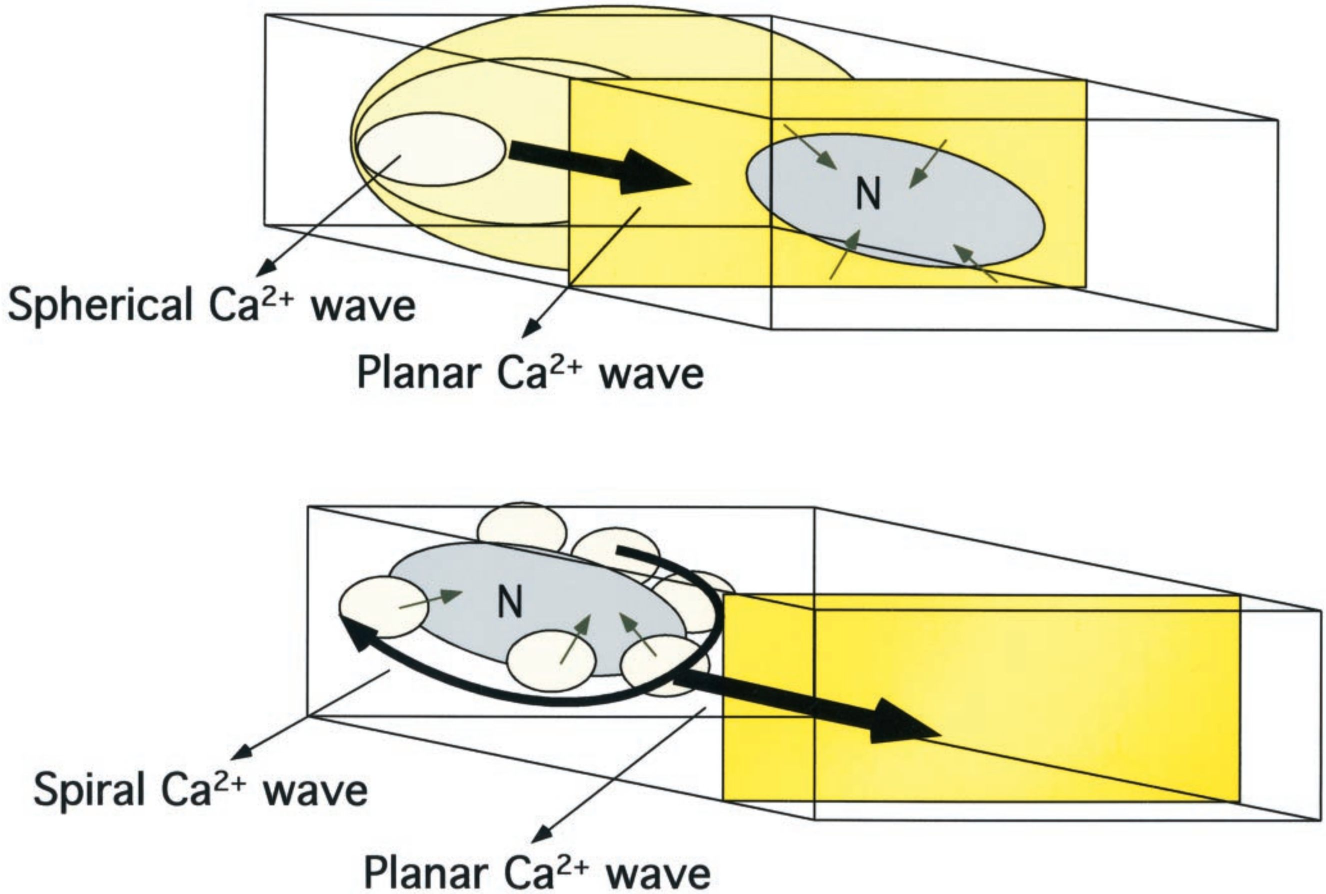

FIGURE 8 Diagram illustrating the influence of the nucleus on spherical and planar Ca^{2+} waves (*top*) and of the importance of the nucleus in the formation of a spiral Ca^{2+} wave (*bottom*).

reticulum (SR); 2) a decrease in a density of Ca^{2+} release channels; or an increase in Ca^{2+} buffering power. We observed that after a spiral Ca^{2+} wave reached the end of nucleus, the Ca^{2+} concentration increased to similar levels observed in planar Ca^{2+} waves (165 ms panel in Fig. 4 and 165 ms panel in *solid circle* in Fig. 5). Therefore, the local increase in Ca^{2+} buffering power provided by the nucleus is likely to contribute to the lower Ca^{2+} concentration and slower propagation of a spiral Ca^{2+} wave. It has been reported that Ca^{2+} can traverse the nuclear membrane by passive diffusion through pores (Lipp and Niggli, 1993; Niggli and Lederer, 1990a). In this study, we observed an increase in nuclear Ca^{2+} concentration due to a planar Ca^{2+} wave (462 ms panel in Fig. 3 and the right side nucleus at 462 ms in Fig. 4) and a spiral Ca^{2+} wave (in the left side nucleus at 363 ms in Fig. 4). Thus the nucleus can buffer Ca^{2+} because Ca^{2+} can diffuse into the nucleus (Genka et al., 1999), but the nucleus has no CICR.

The cytosolic area and nuclear area in cross-section is about 350 and 20 μm^2, respectively (Fig. 2). Therefore, the nucleus occupies only 6% of the area of cross-section in cytosol. Fig. 8 illustrates the importance of these factors. In a planar Ca^{2+} wave, Ca^{2+} is released from SR in all vertical sections so that propagation of a planar Ca^{2+} wave does not change, even though some Ca^{2+} diffuses into the nucleus. If the Ca^{2+} release area is small, however, Ca^{2+} buffering by a nucleus is apparently effective and alters the propagation of Ca^{2+} wave. Therefore, the relationship between the location of a Ca^{2+} wave initiation site and the nucleus is important. If the initial site of the Ca^{2+} wave is close to a nucleus, a spiral Ca^{2+} wave (Fig. 4) may result. However, if the initial origin of a Ca^{2+} wave is not close to a nucleus, a planar Ca^{2+} wave (Fig. 3) will occur.

This work was supported in part by grants-in-aid from the Ministry of Education, Science and Culture of Japan (No. 09877013), from the Tokai University School of Medicine Research Aid, the Nakatani Electronic Measuring Technology Association of Japan, and by National Institutes of Health Grant HL30478.

REFERENCES

Allbritton, N. L., T. Meyer, and L. Stryer. 1992. Range of messenger action of calcium ion and inositol 1,4,5-trisphosphate. *Science*. 258:1812–1815.

Cannell, M. B., H. Cheng, and W. J. Lederer. 1995. The control of calcium release in heart muscle. *Science*. 268:1045–1049.

Dupont, G., J. Pontes, and A. Goldbeter. 1996. Modeling spiral Ca^{2+} waves in single cardiac cells: role of the spatial heterogeneity created by the nucleus. *Am. J. Physiol*. 271:C1390–C1399.

Engel, J., M. Fechner, A. J. Sowerby, S. A. Finch, and A. Stier. 1994. Anisotropic propagation of Ca^{2+} waves in isolated cardiomyocytes. *Biophys. J*. 66:1756–1762.

Fabiato, A. 1985. Time and calcium dependence of activation and inactivation of calcium-induced release of calcium from the sarcoplasmic reticulum of a skinned canine cardiac Purkinje cell. *J. Gen. Physiol*. 85:247–289.

Fabiato, A., and F. Fabiato. 1975. Contractions induced by a calcium-triggered release of calcium from the sarcoplasmic reticulum of single skinned cardiac cells. *J. Physiol. Lond*. 249:469–495.

Fast, V. G., I. R. Efimov, and V. I. Krinsky. 1990. Transition from circular to linear rotation of a vortex in an excitable cellular medium. *Physics Lett. A*. 151:157–161.

Genka, C., H. Ishida, K. Ichimori, Y. Hirota, T. Tanaami, and H. Nakazawa. 1999. Visualization of biphasic Ca^{2+} diffusion from cytosol to nucleus in contracting adult rat cardiac myocytes with an ultra-fast confocal imaging system. *Cell Calcium*. 25:199–208.

Gerhardt, M., H. Schuster, and J. J. Tyson. 1990. A cellular automation model of excitable media including curvature and dispersion. *Science*. 247:1563–1566.

Ichihara, A., T. Tanaami, H. Ishida, and M. Shimizu. 1999. Confocal fluorescent microscopy using a Nipkow scanner. In *Fluorescent and Luminescent Probes*, W. T. Mason, ed. Academic Press. 344–349.

Ishide, N., M. Miura, M. Sakurai, and T. Takishima. 1992. Initiation and development of calcium waves in rat myocytes. *Am. J. Physiol*. 263: H327–H332.

Kagaya, Y., E. O. Weinberg, N. Ito, T. Mochizuki, W. H. Barry, and B. H. Lorell. 1995. Glycolytic inhibition: effects on diastolic relaxation and intracellular calcium handling in hypertrophied rat ventricular myocytes. *J. Clin. Invest*. 95:2766–2776.

Lipp, P., J. Huser, L. Pott, and E. Niggli. 1996. Subcellular properties of triggered Ca^{2+} waves in isolated citrate-loaded guinea-pig atrial myocytes characterized by ratio confocal microscopy. *J. Physiol*. 599–610.

Lipp, P., and E. Niggli. 1993. Microscopic spiral waves reveal positive feedback in subcellular calcium signaling. *Biophys. J*. 65:2272–2276.

Lopez Lopez, J. R., P. S. Shacklock, C. W. Balke, and W. G. Wier. 1995. Local calcium transients triggered by single L-type calcium channel currents in cardiac cells. *Science*. 268:1042–1045.

Niggli, E., and W. J. Lederer. 1990a. Real-time confocal microscopy and calcium measurements in heart muscle cells: toward the development of a fluorescence microscope with high temporal and spatial resolution. *Cell Calcium*. 11:121–130.

Niggli, E., and W. J. Lederer. 1990b. Voltage-independent calcium release in heart muscle. *Science*. 250:565–568.

Nipkow, P. 1884. German Patent No. 30,105.

Petran, M., M. Hadravsky, D. Egger, and R. Galambos. 1968. Tandem-scanning reflected-light microscope. *J. Opt. Soc. Am*. 53:716–718.

Stern, M. D. 1992. Theory of excitation-contraction coupling in cardiac muscle. *Biophys. J*. 63:497–517.

Stern, M. D., M. C. Capogrossi, and E. G. Lakatta. 1988. Spontaneous calcium release from the sarcoplasmic reticulum in myocardial cells: mechanisms and consequences. *Cell Calcium*. 9:247–256.

Takamatsu, T., and W. G. Wier. 1990. Calcium waves in mammalian heart: quantification of origin, magnitude, waveform, and velocity. *FASEB J*. 4:1519–1525.

Tang, Y., and H. G. Othmer. 1994. A model of calcium dynamics in cardiac myocytes based on the kinetics of ryanodine-sensitive calcium channels. *Biophys. J*. 67:2223–2235.

Wier, W. G. 1993. $[Ca^{2+}]_i$ waves in heart cells: more than a passing fancy. *Biophys. J*. 65:2270–2271.

Wong, A., A. Fabiato, and J. Bassingthwaigthe. 1992. Model of calcium-induced calcium release mechanism in cardiac cells. *Bull. Math. Biol*. 54:95–116.

Wussling, M. H., and H. Salz. 1996. Nonlinear propagation of spherical calcium waves in rat cardiac myocytes. *Biophys. J*. 70:1144–1153.